Hierarchical Structures

DOI: 10.1002/ange.200500208

Hierarchical Assembly of {Fe_{13}} Oxygen-Bridged Clusters into a Close-Packed Superstructure**

*Muralee Murugesu, Rodolphe Clérac, Wolfgang Wernsdorfer, Christopher E. Anson, and Annie K. Powell**

Dedicated to Professor Heinrich Vahrenkamp on the occasion of his 65th birthday

Hierarchical materials can be regarded as systems in which small units are incorporated into larger superstructures, thereby investing the resulting construct with a hierarchy of properties that operate on different scales. Such systems become of particular interest when nanometer scales are involved, as these represent a situation in which nanoparticles are organized into a specific array. The organization of nanoparticles is important in terms of creating devices but poses significant difficulties if the particles have to be physically arranged, for example, by using electron-beam lithography. Therefore, the idea of the combination of such particles along chemical principles is attractive as it leaves the chemical-bonding interactions to do the work. Herein, we describe the realization of this idea in a material obtained from aqueous solution and composed of a close-packed superstructure of connected iron(III) nanomagnets, which themselves display close-packed core architectures.

Our conceptual hierarchy begins at the atomic level with Fe^{III} ions in water in the form of the hexaaqua ion $[Fe(H_2O)_6]^{3+}$. Under normal conditions, a variety of hydrolysis reactions would lead to the precipitation of an amorphous hydroxide, which would then age into well-defined mineral phases, such as the oxyhydroxide and goethite phases, and finally transform into the most thermodynamically stable oxide haematite.[1] We have observed that supply of tripodal chelating ligands of the general form $N(RCOOH)_2R'$ (in which R′ can be any organic residue) to such solutions can halt this process through the stabilization of captured intermediate phases composed of close-packed cores, which are portions of the brucite structure (exemplified by $Mg(OH)_2$) encased in a shell of the ligand units.[2,3] It is worth looking at this hydrolysis process in more detail: The brucite structure is an AB_2 lattice composed of close-packed hydroxide (B) layers that are arranged as double strips and M^{II} ions (A) that sit in the octahedral holes between these strips so that each hydroxide unit bridges three metal ions (Figure 1). In the hydrolysis process, we can imagine the

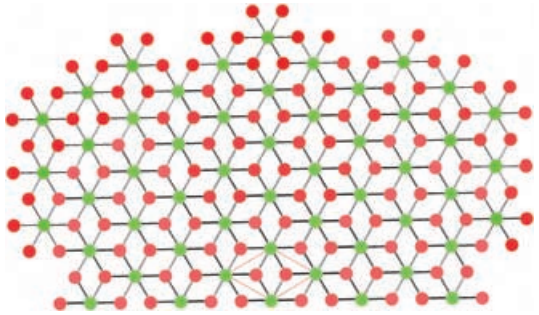

Figure 1. The AB_2 lattice as seen in the brucite $Mg(OH)_2$ structure. Green: metal atoms; red: oxygen atoms.

starting point (first generation) to be a hexaaqua metal ion which will link to six further metal ions (second generation) on production of the hexahydroxo metal ion, and the process will continue through production of the hydroxide ions and coordination to a further six metal centers (third generation), then twelve (fourth generation), and so on, as can be seen in Figure 1.

Aggregates that contain portions of such core structures have been structurally characterized for a variety of metal ions.[2–15] Clearly, an infinite brucite structure is not possible for the examples of M^{III} ions on the basis of charge imbalance, which could be stabilized by the shell of ligands coordinated to the outermost metal ions of the hydroxide lattice in the observed aggregates. A further pertinent point is that removal of half the protons from the double strips of hydroxide moieties in brucite leads to a layer of the α-oxyhydroxide structure, which is exemplified for the Fe^{III} center by goethite, α-FeO(OH), itself the precursor to the most thermodynamically stable phase haematite. Thus, we can think of such aggregates as metastable intermediates that are trapped through the process of crystallization. These aggregates prove to be magnetically interesting for the Fe^{III} center because, although the overall coupling is antiferromagnetic, the pairwise interactions are unequal in magnitude over the whole molecule, thus leading to residual ground-state spins of up to 33/2 and a display of hysteresis of the magnetization.[3,16–18] Thus, a secondary level of organization both in terms of the structure and properties of the compound is demonstrated. In the specific case we describe herein, the tripodal proligand nitrilotripropionic acid ($H_3ntp = N(CH_2CH_2COOH)_3$) has been used to successfully trap {Fe_{13}} aggregates (Figure 2), in which the production of the

[*] Dr. M. Murugesu, Dr. C. E. Anson, Prof. A. K. Powell
Institut für Anorganische Chemie der Universität Karlsruhe
Engesserstrasse Geb. 30.45
76128 Karlsruhe (Germany)
Fax: (+49) 721-608-8142
E-mail: powell@chemie.uni-karlsruhe.de
Dr. R. Clérac
Centre de Recherche Paul Pascal
CNRS-UPR 8641, 115 Avenue Dr. A. Schweitzer
33600 Pessac (France)
Dr. W. Wernsdorfer
Laboratoire Louis Neél, CNRS
25 Avenue Des Martyrs BP166
38042 Grenoble Cedex 9 (France)

[**] This work was supported by the DFG through the Schwerpunkt Programm SPP 1137 on "Molecular Magnetism", the Center for Functional Nanostructures (CFN), the Conseil Régional d'Aquitaine, Bordeaux I University, and the CNRS.

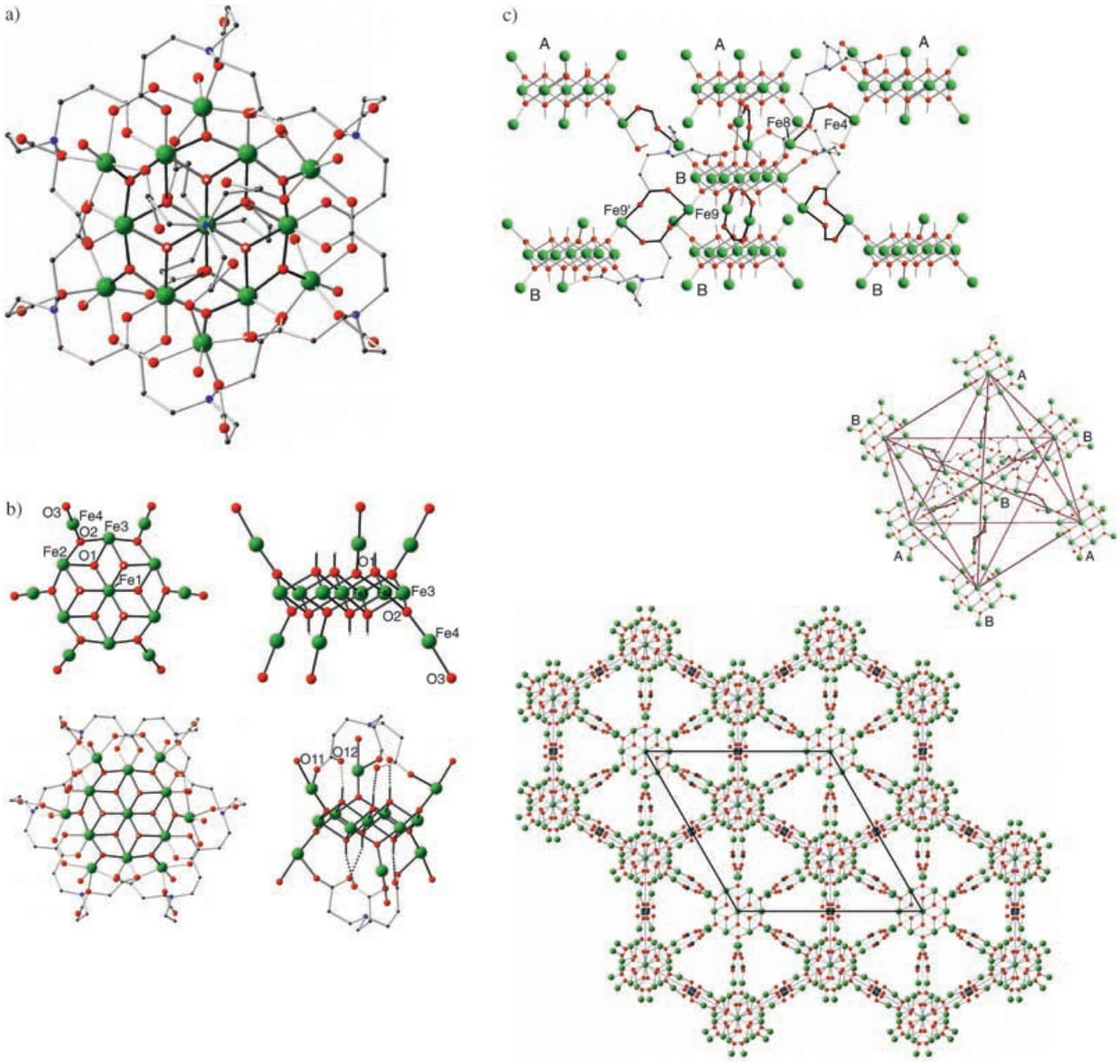

Figure 2. The structural features of the $\{Fe_{13}\}$ aggregate. a) One complete $[Fe_{13}(\mu_3\text{-}OH)_6(\mu_3\text{-}O)_6(H_2O)_6(Hntp)_8]^{5+}$ cluster. b) Top and side views of the $[Fe_{13}(\mu_3\text{-}OH)_6(\mu_3\text{-}O)_6(H_2O)_6]^{21+}$ core in $[Fe_{13}(\mu_3\text{-}OH)_6(\mu_3\text{-}O)_6(H_2O)_6(Hntp)_8]^{5+}$ and the coordination of the $Hntp^{2-}$ ligands to this core. c) The connections between the **A**- and **B**-type clusters; linkage of a **B**-type cluster with its six surrounding neighbors showing the octahedral arrangement of the clusters; and the 3D packing arrangement of the compound viewed down the *c* axis (most of the ligand atoms have been omitted for clarity). Fe green; O red; N blue; C black; H white.

brucite lattice has effectively been arrested at the third generation.

The iron–oxygen framework is shown in Figure 2b, which shows that the central core of the $[Fe_7(OH)_6]^{15+}$ ion clearly corresponds to the first two generations of the brucite lattice and that the final six Fe^{III} centers of the third generation are connected to this core by six triply bridging oxide rather than hydroxide ions. These oxides provide an important structural element as they link three metal ions in a trigonal rather than pyramidal fashion. This coordination mode has the result that the final six iron centers are disposed above and below the core, thus alternating with the hydroxide units to give a "diabolo" arrangement, and means that the iron centers form a trigonal-antiprismatic arrangement, which becomes important in the quaternary structure.

The proligand H_3ntp did not coordinate to the aggregate in the tripodal chelation mode as expected and as seen in the $\{Cu_{44}\}$ compound we recently reported[19] because the central nitrogen atom carries a proton and, therefore, does not form bonds with the peripheral iron centers. This coordination mode has, however, been observed by us in some different Cu^{II} compounds.[20] Consequently, the carboxylate groups are not constrained to form chelate rings, and so the carboxylate functionalities from six ligands display extensive bridging interactions around the periphery of the molecule. Two further ligands complete the encapsulation of the iron core by

capping above and below, with coordination to the peripheral iron centers from the carboxylate groups and hydrogen-bonding interactions between the non-coordinated carboxylate oxygen atoms and the hydroxide functionalities in the core. The proton on the central nitrogen atom of each ligand also forms hydrogen-bonding interactions with the carboxylate oxygen atoms in a trifurcated fashion. The resulting structure is nearly spherical, with a diameter of about 1.5 nm. The positive charge of 5+ on the aggregate (the ligand is dinegative in this zwitterionic form) is balanced in the crystal structure by nitrate counterions. In fact, there are two almost identical aggregates, $[Fe_{13}(\mu_3\text{-}OH)_6(\mu_3\text{-}O)_6(Hntp)_8(H_2O)_6]^{5+}$ (cluster **A**; $Hntp = HN(CH_2CH_2COO)_3$) and $[Fe_{13}(\mu_3\text{-}OH)_6(\mu_3\text{-}O)_6(Hntp)_8]^{5+}$ (cluster **B**), in a 1:2 ratio in the three-dimensional structure. The subtle difference between these clusters becomes clear when the structure is examined in detail: In the third level of organization, the **A**-type clusters are linked to the **B**-type clusters by a *syn–anti* carboxylate bridge from a ligand located on **A** which connects a peripheral Fe^{III} center in **A** to a peripheral Fe^{III} center in **B**. In addition, the **B**-type clusters are linked to each other through double *syn–anti* carboxylate bridges (Figure 2c).

The molecules are arranged in layers that correspond to an ABBABBABBA ordering. A closer examination of the packing reveals the consequences of the arrangement of the peripheral Fe^{III} centers in the trigonal antiprismatic geometry and the fourth level of organization. As a result of the links between the aggregates that arise from ligands coordinated to these iron centers, each aggregate is octahedrally surrounded by six further aggregates (Figure 2c); therefore, for a given **A** aggregate there are six **B** aggregates, whereas for a **B** aggregate there are three **A** and three further **B** aggregates that assume three facial positions of the octahedral "coordination" geometry in each case. The overall result for the organization of the aggregates can be visualized as the interpenetration of *pseudo*-cubic lattices, which is exemplified by the sodium chloride structure. The fact that this organization is actually an AB_2 structure complicates the description slightly, but if we refer back to the brucite structure shown in Figure 1, in which the green and red spheres now represent the **A** and **B** clusters, respectively, the hierarchical nature of this material becomes clear. The unit cell marked in Figure 1 corresponds to the unit cell for our compound (also marked in Figure 2c). In this way, nanoscale aggregates with cores of close-packed atoms with an AB_2 structure have been organized into a close-packed AB_2 superstructure. It is of particular note that within the cores of the aggregates we see Fe^{III} centers that occupy octahedral holes between two layers of close-packed hydroxide moieties and in the superstructure we have **A** clusters that occupy octahedral sites between two layers of **B** clusters.

The question now arises as to whether this hierarchical structure is reflected in the magnetic properties of the material. The plot of χT versus T decreases continuously over the whole temperature range studied from 16.5 emu K mol^{-1} at 300 K to 4.11 emu K mol^{-1} at 30 K (Figure 3). Below this temperature, the χT product decreases faster to reach 1.37 emu K mol^{-1} at 1.8 K. The χT value at room temperature is well below the expected value (56.9 emu K mol^{-1}, if $g = 2$)

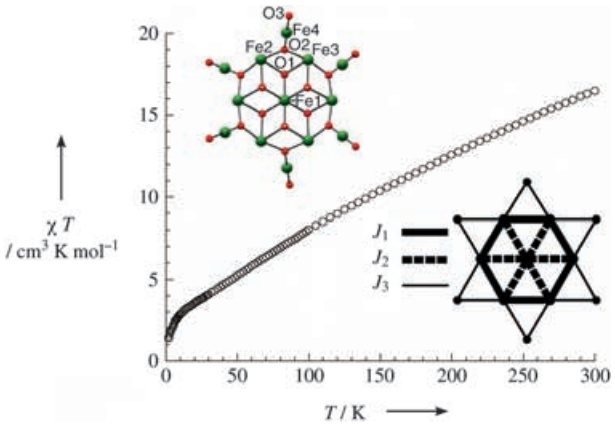

Figure 3. Temperature dependence of the χT product (per Fe^{III} aggregate) at 1000 Oe. Inset: Topology of the magnetic interactions in the iron aggregates.

for 13 high-spin Fe^{III} centers ($S = 5/2$), thus indicating strong antiferromagnetic interactions between the centers.

A simplified scheme of the magnetic-interaction topology based on the coordination modes between the Fe^{III} centers can be proposed (inset Figure 3) with three types of pathway: J_1 coupling through the μ_3-O and μ_3-OH double bridges, J_2 coupling through the μ_3-OH double bridges, and J_3 coupling through the single μ_3-O bridges. All of these exchange couplings are known to lead to antiferromagnetic interactions. Therefore, the topology and the symmetry of the $\{Fe_{13}\}$ aggregates (inset Figure 3) reveal the presence of a triangular assembly, with a competing set of antiferromagnetic interactions. Modeling the magnetic susceptibility is not possible as 1) there is no analytical model available for 13 coupled Fe^{III} centers in such a configuration and 2) numerical methods would require the diagonalization of too large a matrix. However, numerical density functional theory calculations on $[Fe_{19}(metheidi)_{10}(\mu_3\text{-}OH)_6(\mu\text{-}OH)_8(\mu_3\text{-}O)_6(H_2O)_{12}]NO_3$ ($H_3metheidi = N(CH_2COOH)_2(CH(Me)CH_2CH_2OH)$), a molecule with the same brucite-core structure as seen in the $\{Fe_{13}\}$ aggregate,[21] were recently used to evaluate Fe^{III}–Fe^{III} magnetic coupling through different types of oxygen bridges. Herein, we suggest that the J_3 coupling through the μ_3-O bridge will be the strongest and will occur at around −100 K and that the J_2 coupling should be almost half of the J_1 coupling (namely, around −10 K compared with −20 K). Therefore, a simple view of the ground state can be proposed based on this coupling scheme in which all the outermost spins are parallel to each other and antiparallel to the spins on their neighbors that make up the middle ring. Finally, the J_2 coupling results in the spin on the central Fe center being antiparallel to these neighboring spins and, thus, parallel to the outermost spins, which would result in a spin ground state for the $\{Fe_{13}\}$ aggregates of 5/2.

Low-temperature measurements give further insight into the ground state and the anisotropy of the $\{Fe_{13}\}$ units. The fact that the χT product does not go directly to zero at low temperature indicates that it is not a singlet ground state, as to be expected for an odd number of antiferromagnetically coupled spin carriers. The value reached at 30 K is 4.1 emu K

mol^{-1}, which is compatible with a ground state of $S = 5/2$. The further decrease of the χT product at lower temperature is probably because of the intercluster interactions mediated by the *syn–anti* carboxylate bridges, a zero-field-splitting contribution, or both of these. This interpretation is confirmed by the field dependence of the magnetization at 1.8 K (Figure 4a). Two regimes are observed: 1) at low field below 1 T,

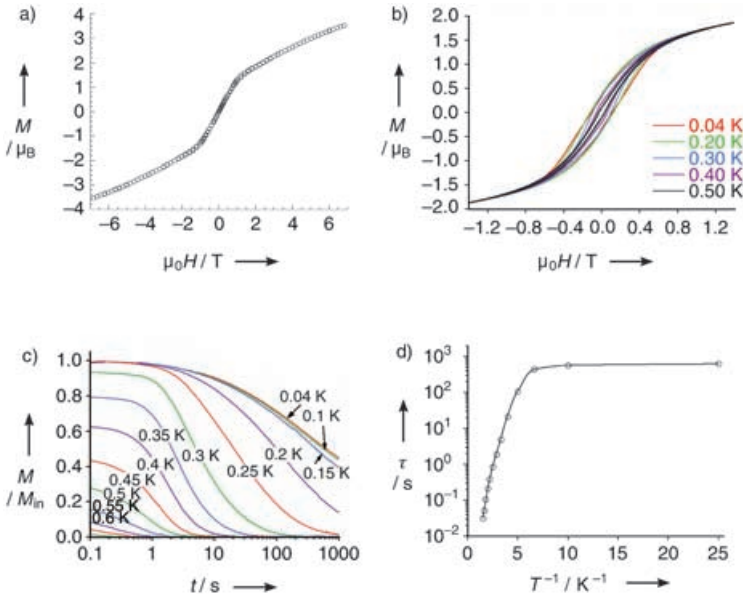

Figure 4. a) Bulk-field dependence of the magnetization (per Fe^{III} aggregate) at 1.83 K and b) field dependence of the magnetization on a single crystal from 0.04 to 0.5 K by the micro-SQUID technique with the magnetic field applied along the *c* axis. c) Relaxation of the magnetization below 0.7 K normalized to the initial magnetization at 0.04 K by the micro-SQUID technique with the magnetic field applied along the *c* axis. d) Plot of relaxation time τ versus $1/T$.

where the magnetization increases rapidly and linearly, and 2) above 1 T, where the increase is slower. Although saturation is not achieved at 7 T, the nonlinear behavior indicates that the saturation should be achievable at higher fields and have a value probably close to 5 μ_B, which is to be expected for a ground state of $S = 5/2$. The presence of these two regimes may be the result of the anisotropy and/or the interactions between the aggregates; therefore, micro-SQUID measurements were performed on a single crystal at temperatures lowered to 0.04 K for yet further insight into the magnetic behavior. This technique and rotation of the applied field around the single crystal shows that the measured magnetization becomes clearly uniaxially anisotropic below 2 K, thus implying a negative value of *D*. Furthermore, below 1 K and when the applied field does not coincide with the *c* direction, the curves for *M* versus *H* exhibit a characteristic S shape that is typical for antiferromagnetically coupled systems with an inflexion point at around 0.6 T at 40 mK. Therefore, these two simple observations demonstrate that both anisotropy and interaggregate interactions are relevant in the low-temperature regime. Hysteresis loops are observed below 1 K with the largest effect seen when the field coincides with the *c* axis, thus suggesting that this effect corresponds to the easy axis (Figure 4b). Although the loops do not show a large temperature dependence, we can rule out the possibility that they result from a spin-glass behavior from the temperature dependence of the magnetization relaxation time. In a classical spin-glass system, the relaxation time follows what looks like an Arrhénius behavior but with nonphysical values for the energy barrier and the pre-exponential factor,[22] which is, in fact, not the case, as seen in Figure 4d.

As the curves for M/M_{in} versus t (M/M_{in} is the magnetization normalized to its initial value at 0.04 K) obtained below 0.7 K have the same shape (Figure 4c), the data were scaled to a single master curve and the relaxation time τ was extracted by simply taking the time when M/M_{in} reaches the value $1/e$ (Figure 4d). The relaxation time for the high-temperature section of the plot of τ versus $1/T$ does not follow the simple Arrhénius behavior expected for single-molecule magnets (SMM) in the thermally activated regime. This nonexponential behavior is probably a result of the magnetic interactions between the $\{Fe_{13}\}$ aggregates and suggests that these units when isolated from each other would behave as SMMs. Below 0.1 K, saturation of τ is reached, thus indicating that the dominant process of relaxation becomes time independent. This feature is reminiscent of SMM behavior when quantum tunneling of the magnetization is the main pathway for the relaxation. In our case, the slow relaxation of the magnetization is induced necessarily not only by the spin ground state and the anisotropy of the $\{Fe_{13}\}$ aggregates but also by the significant three-dimensional antiferromagnetic coupling between them. This result illustrates the influence of the hierarchical structure of this compound and the role of the chemical and magnetic coupling between the $\{Fe_{13}\}$ aggregates that give rise to a hierarchy of magnetic properties.

Although further work needs to be carried out on the physics of this complicated system, it is clear that by physically connecting the spins of the aggregates with chemical bonds, cooperative interaction at low temperature has been enabled, thus giving rise to the exotic effects observed. Overall, we feel that this system is fascinating both in terms of the aesthetic appeal of the structural concepts and its potential to provide detailed insight into magnetic interactions between nanoscale particles.

Experimental Section

$[\{Fe_{13}(\mu_3\text{-}OH)_6(\mu_3\text{-}O)_6(Hntp)_8(H_2O)_6\}\{Fe_{13}(\mu_3\text{-}OH)_6(\mu_3\text{-}O)_6(Hntp)_8\}_2]\cdot 15NO_3\cdot 13H_2O$ (**1**): A solution of H_3ntp (0.058 g, 0.25 mmol) and ethylenediamine (0.017 mL, 0.25 mmol) in H_2O (5 mL) was added to a solution of $[Fe(NO_3)_3]\cdot 9H_2O$ (0.202 g, 0.5 mmol) in H_2O (5 mL) with stirring. Vapor diffusion of EtOH into the resulting brown solution gave red–brown diamond-shaped crystals after three weeks (17% yield). Elemental analysis (%) calcd for $C_{216}H_{444}Fe_{39}N_{39}O_{282}$: C 25.24, H 4.35, N 5.31; found: C 25.23, H 4.03, N 5.38.

Crystal structure data for **1**: $C_{216}H_{450}Fe_{39}N_{39}O_{244}$, $M_r = 9676.2$; trigonal, $P\bar{3}c1$, $a = 24.2756(12)$, $c = 35.4381(19)$ Å, $U = 18085.9(16)$ Å^3, $Z = 4$, $T = 200$ K, $\rho_{calcd} = 1.777$ Mg m^{-3}, $\mu = 1.647$ mm^{-1}; Stoe IPDS area detector diffractometer with graphite-monochromated $Mo_{K\alpha}$ radiation; 105539 reflections measured, 13313

unique, $R_{int} = 0.1290$, $2\theta_{max} = 56.3°$, 99.8% completeness, wR_2(all data) = 0.2134, $R_1 = 0.0829$ using 8706 reflections with $I \geq 2\sigma(I)$, parameters/restraints 884/50, residual electron density +0.86/−0.93; semiempirical absorption correction by using XPREP in SHELXTL;[22] structure solution by direct-methods and full-matrix least-squares refinement against F^2 (all data) by using SHELXTL;[23] anisotropic refinement for all non-hydrogen atoms except for some minor disorder components, hydrogen atoms isotropic. CCDC-260817 contains the supplementary crystallographic data for this paper. These data can be obtained free of charge from the Cambridge Crystallographic Data Center via www.ccdc.cam.ac.uk/data_request/cif.

Magnetic susceptibility measurements on **1** were obtained on a finely ground polycrystalline sample (5.9 mg) using a Quantum Design SQUID magnetometer MPMS-XL. The dc measurements were collected from 1.8 to 300 K and from −70 to 70 kOe. Experimental data were also corrected for the sample holder and for the diamagnetic contribution calculated from Pascal constants.[24] Field and time dependences of the magnetization on single crystals were measured with an array of micro-SQUIDs.[25]

Received: January 19, 2005
Revised: June 14, 2005
Published online: September 27, 2005

Keywords: cluster compounds · coordination modes · hierarchical structures · iron · magnetic properties

[1] R. M. Cornell, U. Schwertmann, *The Iron Oxides*, VCH, Weinheim, **1996**.
[2] S. L. Heath, A. K. Powell, *Angew. Chem.* **1992**, *104*, 191; *Angew. Chem. Int. Ed. Eng.* **1992**, *31*, 191.
[3] J. C. Goodwin, R. Sessoli, D. Gatteschi, W. Wernsdorfer, A. K. Powell, S. L. Heath, *J. Chem. Soc. Dalton Trans.* **2000**, 1835.
[4] M. A. Bolcar, S. M. J. Aubin, K. Folting, D. N. Hendrickson, G. Christou, *Chem. Commun.* **1997**, 1485.
[5] M. Tesmer, B. Müller, H. Vahrenkamp, *Chem. Commun.* **1997**, 721.
[6] G. L. Abbati, A. Cornia, A. C. Fabretti, A. Caneschi, D. Gatteschi, *Inorg. Chem.* **1998**, *37*, 3759.
[7] H. Oshio, N. Hoshino, T. Ito, M. Nakano, F. Renz, P. Gütlich, *Angew. Chem.* **2003**, *115*, 233; *Angew. Chem. Int. Ed.* **2003**, *42*, 223.
[8] S. Boulmaaz, R. Papiernik, L. G. Hubertpfalzgraf, J. Vaissermann, J. C. Daran, *Polyhedron* **1992**, *11*, 1331.
[9] I. A. M. Pohl, L. G. Westin, M. Kritikos, *Chem. Eur. J.* **2001**, *7*, 3438.
[10] J. T. Brockman, J. C. Huffman, G. Christou, *Angew. Chem.* **2002**, *114*, 2616; *Angew. Chem. Int. Ed.* **2002**, *41*, 2506.
[11] M. Murrie, H. Stoeckli-Evans, H. U. Güdel, *Angew. Chem.* **2001**, *113*, 2011; *Angew. Chem. Int. Ed.* **2001**, *40*, 1957.
[12] E. K. Brechin, S. G. Harris, A. Harrison, S. Parsons, A. G. Whittaker, R. E. P. Winpenny, *Chem. Commun.* **1997**, 653.
[13] J. C. Goodwin, S. J. Teat, S. L. Heath, *Angew. Chem.* **2004**, *116*, 4129; *Angew. Chem. Int. Ed.* **2004**, *43*, 4037.
[14] S. L. Heath, P. A. Jordan, I. D. Johnson, G. R. Moore, A. K. Powell, M. Helliwell, *J. Inorg. Biochem.* **1995**, *59*, 785.
[15] W. Schmitt, E. Baissa, A. Mandel, C. E. Anson, A. K. Powell, *Angew. Chem.* **2001**, *113*, 3689; *Angew. Chem. Int. Ed.* **2001**, *40*, 3578.
[16] A. K. Powell, S. L. Heath, D. Gatteschi, L. Pardi, R. Sessoli, G. Spina, F. Del Giallo, F. Pieralli, *J. Am. Chem. Soc.* **1995**, *117*, 2491.
[17] D. J. Price, F. Lionti, R. Ballou, P. T. Wood, A. K. Powell, *Philos. Trans. R. Soc. London Ser. A* **1999**, *357*, 3099.
[18] M. Affronte, R. Sessoli, D. Gatteschi, W. Wernsdorfer, J. C. Lasjaunias, S. L. Heath, A. K. Powell, A. Fort, A. Rettori, *J. Phys. Chem. Solids* **2004**, *65*, 745.
[19] M. Murugesu, R. Clérac, C. E. Anson, A. K. Powell, *Inorg. Chem.* **2004**, *43*, 7269.
[20] M. Murugesu, R. Clérac, C. E. Anson, A. K. Powell, *J. Phys. Chem. Solids* **2004**, *65*, 667.
[21] E. Ruiz, A. Rodríguez-Fortea, J. Cano, S. Alvarez, *J. Phys. Chem. Solids* **2004**, *65*, 799.
[22] J. A. Mydosh, *Spin Glasses: An Experimental Introduction*, Taylor and Francis, London, **1993**.
[23] G. M. Sheldrick, SHELXTL 5.1, Bruker AXS Inc., 6300 Enterprise Lane, Madison, WI 53719-1173, USA, **1997**.
[24] E. A. Boudreaux, L. N. Mulay, *Theory and Applications of Molecular Paramagnetism*, Wiley, New York, **1976**.
[25] W. Wernsdorfer, *Adv. Chem. Phys.* **2001**, *118*, 99.

